

# Time Dependent Modeling of the Markarian 501 X-ray and TeV Gamma-Ray Data Taken During March and April, 1997

H. Krawczynski<sup>1</sup>, P.S. Coppi<sup>1</sup>, F. Aharonian<sup>2</sup>

<sup>1</sup> *Yale University, P.O. Box 208101, New Haven, CT 06520-8101, USA*

<sup>2</sup> *Max Planck Institut für Kernphysik, Postfach 103980, D-69029 Heidelberg, Germany*

Accepted — —. Received 2002, January 21

## ABSTRACT

If the high-energy emission from TeV blazars is produced by the Synchrotron Self-Compton (SSC) mechanism, then simultaneous X-ray and Gamma-ray observations of these objects are a powerful probe of the electron (and/or positron) populations responsible for this emission. Understanding the emitting particle distributions and their evolution in turn allow us to probe physical conditions in the inner blazar jet and test, for example, various acceleration scenarios. By constraining the SSC emission model parameters, such observations also allow us to predict the intrinsic (unabsorbed) Gamma-ray spectra of these sources, a major uncertainty in current attempts to use the observed Gamma-ray spectra to constrain the intensity of the extragalactic background at optical/infrared wavelengths. Although the time-averaged spectral energy distribution (SED) of blazars like Mrk 421 and Mrk 501 is consistent with SSC predictions, this is not a definitive test of the SSC model since other models can also reproduce the SED. The observed emission is in fact extremely variable and time-averaging discards significant information making the interpretation of the results ambiguous. As a next step in testing the SSC model and as a demonstration of the potential power of coordinated X-ray and Gamma-ray observations, we attempt to model in detail the X-ray and Gamma-ray light curves of the TeV blazar Mrk 501 during its April-May 1997 outburst using a simple time dependent SSC emission model. Extensive, quasi-simultaneous X-ray and Gamma-ray coverage exists for this period, and the flaring activity is so intense and rapid during this time that only one emission region is likely to be active during a given flare. We discuss and explore quantitatively several of the flare scenarios presented in the literature. We show that simple two-component models (with a soft, steady X-ray component plus a variable SSC component) involving substantial pre-acceleration of electrons to Lorentz factors on the order of  $10^5$  describe the data train surprisingly well. All considered models imply an emission region that is strongly out of equipartition and a low radiative efficiency of  $\lesssim 10^{-3}$ . Degeneracy in both, model variant and jet parameters, prevents us to use the time resolved SSC calculations to substantially tighten the constraints on the amount of TeV Gamma-ray extinction by the Diffuse Extragalactic Background Radiation (DEBRA), compared to earlier work.

**Key words:** galaxies: BL Lacertae objects: individual (Mrk 501) — galaxies: jets — X-rays: galaxies — gamma rays: theory

## 1 INTRODUCTION

### 1.1 EGRET Blazar Observations

The EGRET detector on board the *Compton Gamma-Ray Observatory* showed that many blazars are copious Gamma-ray emitters (Hartman et al. 1999), their power at Gamma-ray energies being comparable to (for low luminosity sources,

i.e. BL Lac objects) or dominating by a wide margin (for high luminosity sources, i.e., FSRQs, Flat Spectrum Radio Quasars, and OVV, Optically Violantly Variables) the power emitted at longer wavelengths. The nonthermal radiation component probably originates from a population of relativistic particles embedded in the collimated, relativistic outflow (jet) from a super-massive ( $10^6$  up to sev-

eral times  $10^9 M_\odot$ ). The nonthermal continuum emission is commonly explained with Synchrotron Compton (SC) models (see e.g., Ulrich et al. 1997): embedded in a jet which approaches the observer with a relativistic velocity, a population of high energy electrons emits Synchrotron radiation at longer wavelengths and at shorter wavelengths, Inverse Compton (IC) radiation of high energy electrons off lower energy seed photons. The origin of the seed photons is a matter of considerable uncertainty and debate (e.g., see Błażejowski et al. (2000)). The seed photon source could be “external” to the jet, e.g., radiation scattered and re-processed by ambient matter in the so-called Broad Line Region near the black hole, or infrared radiation emitted by dust in the inner nucleus of the host galaxy. Alternatively, the seed photon source could be “internal” to the jet. In the simplest case (the SSC model), the dominant seed photons are synchrotron photons from the same electron population responsible for the IC scattering. In a generic source, both external and internal seed photons could be important in producing the observed spectrum. Alternative models, so-called “hadronic” models, invoke hadronic interactions of a highly relativistic outflow which sweeps up ambient matter (Pohl & Schlickeiser 2000), interactions of high energy protons with gas clouds moving across the jet (Dar & Laor 1997), or, interactions of extremely high energy protons with ambient photons (Mannheim 1998), with the jet magnetic field (Aharonian 2000), or with both (Mücke & Protheroe 2000).

All these models have some degree of success in explaining the overall spectral energy distribution (SED) of Gamma-ray blazars. However, one can break much of the apparent degeneracy between these models by taking advantage of the rapid, large-scale time variability these sources exhibit. Different models, for example, produce emission at a given frequency using particles of different energies, interaction cross-sections, and cooling times. The response of different models to changes in source conditions or the injection of fresh new particles is therefore different and in principle distinguishable – provided that one has sufficient time resolution to fully sample the flux variations and sufficient frequency coverage to constrain the different emission components that may be present.

In view of this potential payoff, considerable effort has been dedicated to carrying out multi-wavelength observations on powerful EGRET blazars like 3C 279 (Wehrle et al. 1998). While the campaigns have lent considerable support to the SC model hypothesis, the results of the campaigns were not as conclusive as one might have hoped. The reasons for this are three-fold:

(i) These blazars turned out to be highly variable on timescales down to at least hours (Mattox et al. 1997; Wagner et al. 1997). Even for the brightest objects, the instrument available for the Gamma-ray observations, EGRET, simply did not have enough collection area to track all the Gamma-ray flux variations, let alone provide high quality energy spectra.

(ii) In typical SC models the electrons responsible for the GeV EGRET IC flux emit their synchrotron radiation at  $\sim$ UV energies. However, UV observations are difficult if not impossible because of atmospheric and galactic absorption. Thus the simultaneous observations that were made, e.g.,

at Gamma-ray and X-ray energies, tracked radiation from electrons with very different energies and different cooling times and thus potentially different time histories and perhaps even emission regions.

(iii) The observations showed that the Gamma-ray emission in several EGRET blazars is not consistent with the SSC model, the simplest version of SC models (see e.g. the comprehensive modeling of 3C 279 broadband data described by Hartman et al. 2001). The necessity to consider in so-called “External Compton” (EC) models alternative seed photon fields substantially complicates the unambiguous interpretation of the data, especially since along our line of sight the beamed emission from the jet often dominates, making direct observation of these other photon fields difficult.

## 1.2 Potential of TeV Blazar Observations

The second class of Gamma-ray emitting blazars that EGRET discovered, the low power BL Lac objects like Mrk 421, were initially passed over as targets for extensive multi-wavelength campaigns since they were too weak in the EGRET band. The arrival of ground-based Gamma-ray detectors like Whipple, HEGRA, and CAT with detection areas on the order of  $10^5 \text{ m}^2$ , however, now allows us to follow their Gamma-ray fluxes on minute timescales (Gaidos et al. 1996) and to routinely obtain detailed spectral information on timescales down to one hour (Aharonian et al. 1999a). Besides their better accessibility at Gamma-ray energies, these low power objects have several other important advantages. BL Lacs and their likely FR-1 radio galaxy parent population appear to have underluminous accretion disks, i.e., “external” photon fields may not be important as seeds for IC scattering (Chiaberge et al. 1999). This together with the fact that their time-averaged SEDs have successfully been described with one-component SSC models, strongly suggests that SSC which have much fewer free parameters than External Compton models indeed apply. Also, perhaps because of the lower internal and external radiation fields and thus lower radiative losses (Ghisellini et al. 1998), the characteristic electron energies appear to be higher for the lower power objects, moving their synchrotron emission peak out of the UV squarely into the X-ray range, where individual flares strongly dominate the overall luminosity and can readily be observed with broad-band X-ray satellites like RXTE and BeppoSAX. In the SSC model, the IC peak then moves from GeV to  $\sim$ TeV energies. Thus, simultaneous X-ray and TeV Gamma-ray observations follow the evolution of the electron population responsible for the bulk of the source luminosity, and the observations are well-matched in the sense that they track the emission from the *same* electrons, providing tight constraints on the electron distribution and its time evolution. SSC models that apply to these objects are therefore testable, especially with the next generation of X-ray and Gamma-ray detectors coming on line in the next few years. Proving whether an SSC model works or not has a potentially large payoff. If the model does not work, then we must significantly revise our understanding of the physical conditions and processes in these object. If it does work, then we can use it for example to probe the acceleration processes at work in the innermost region of the jet. We can also use it to constrain the amount of

extragalactic Gamma-ray extinction due to pair production processes on the diffuse optical/infrared background  $\gamma_{\text{TeV}} + \gamma_{\text{IR},o} \rightarrow e^+ e^-$  (Gould & Schröder 1966; Stecker, De Jager & Salamon 1992), by comparing the predicted intrinsic TeV Gamma-ray energy spectrum with the observed one (Coppi & Aharonian 1999, Krawczynski et al. 2000, called “Paper I” in the following”).

Based on these considerations, the brightest TeV blazars, Mrk 421 ( $z = 0.031$ ) and Mrk 501 ( $z = 0.034$ ), have been the subject of increasingly intensive observing campaigns. This has led to the discovery of pronounced TeV Gamma-ray / X-ray flux correlations for Mrk 421 (Buckley et al. 1996; Takahashi et al. 1996) and Mrk 501 (Pian et al. 1998, Djannati-Atai et al. 1999, Paper I, Sambruna et al. 2000, see also Fig. 1).

### 1.3 Goal of this Paper and Relation to Previous Work

The goal of this paper is to extend the analysis of Paper I, which was a first joint X-ray/TeV analysis of the unprecedented set of monitoring data taken during the April-May 1997 flare of Mrk 501. Using RXTE (X-ray) and HEGRA (TeV) observations that were simultaneous to within a few hours (i.e. less than the  $\sim 12$  hour characteristic variability time scale of the source), we showed that the X-ray flux of the source, particularly above 10 keV, was strongly correlated with the TeV/X-ray flux, in accord with SC models. Moreover, we found that for that two month period TeV flux variations were consistent with the quadratic relation expected between the X-ray and TeV flux in a simple SSC model, although a linear relation between X-ray and TeV flux plus a constant base X-ray flux level also described the data relatively well. We then used a one-zone, steady state SSC model to fit the average X-ray/Gamma-ray spectra for several days in order to see if the model could explain the data and to make a first guess at the SSC source parameters. We found that the data could be fairly well-described by a reasonable sequence of SSC models. By assuming that we were indeed seeing SSC emission and by taking (at the time) extreme values of the SSC model parameters (e.g., jet Doppler factors  $\sim 100$ ), we then placed constraints on the maximum amount of extragalactic Gamma-ray absorption present in the observed spectrum (Paper I, Fig. 10). Since that paper, theoretical and observational estimates of the diffuse infrared and optical backgrounds have increased significantly and are now barely consistent with the constraints of Paper I (e.g., see Primack et al. 2001). We will give an updated discussion of the implications of SSC and EC models on the intensity of the diffuse extragalactic background radiation in a companion paper (Coppi et al. 2001).

In this paper, we attempt to quantify how well SSC model predictions match observations by taking the 1997 data set and fitting the full observed spectral sequence using a time dependent SSC code (Coppi 1992). The code accurately models the temporal evolution of the energy distribution function of a population of relativistic electrons due to acceleration processes and radiative and adiabatic energy losses. However, it is a one-zone code that assumes homogeneous and isotropic particle and pitch angles distributions in the jet rest frame. Leaving aside plasma and magnetohydrodynamics issues, such assumptions are clearly

an oversimplification given the inhomogeneous structure of jets, especially as observed on VLBI radio scales where several distinct “blobs” (emission regions) may be active at any given time. However, during 1997 the Mrk 501 emission was strongly dominated by individual flares during which the X-ray flux increased by factors of up to 5 and the TeV Gamma-ray fluxes by factors up to 30. It is highly probable these individual flares were produced by single jet regions, rather than being the superposition of several causally not connected events. Note that in addition, the physical conditions in all the emission regions seemed to be very similar: the X-ray and TeV Gamma-ray fluxes were well correlated during more than two months (see Paper I, and this paper Fig. 1), and the TeV energy spectrum stayed remarkably stable during more than 6 months (Aharonian 1999a-c).

Observational signatures of synchrotron Compton models have been described by various authors (see e.g. the references given in Table 1). In the following we show for the first time an attempt to fit a prolonged sequence of X-ray and TeV Gamma-ray data with a time dependent SSC code. This approach makes it possible to use the full information encoded in the correlated flux variability at different wavelengths. In contrast to parametric SSC fits (see e.g. Paper I, Tavecchio et al. 2001) the method uses a self-consistently evolved electron population which assures that the assumed electron energy spectrum is physically realizable from an initial acceleration spectrum (see also the discussion by Mastichiadis & Kirk 1997). We think that the approach of using a time resolved analysis to break model degeneracies will become increasingly more powerful and important as the sensitivity and energy coverage of X-ray and Gamma-ray instruments continue to improve. Note that a thorough understanding of the SSC model is also a necessary prerequisite for the evaluation of EC models which always include a SSC component.

The rest of this paper is structured as follows. In Sect. 2 we introduce the data set and show an updated version of the X-Ray/TeV Gamma-ray flux correlation. In Sect. 3 we describe the model calculations and in Sect. 4 the time dependent model fits. Finally, we discuss the results in Sect. 5.

## 2 THE DATA SET

During 1997 the BL Lac object Mrk 501 went into a remarkable state of continuous strong flaring activity and the source was intensively monitored at X-rays and TeV Gamma-rays during this year. During April and May, 1997 the source was regularly observed with the RXTE X-ray satellite, with typically two pointed observations per day of  $\sim 20$  min duration (Paper I). Each pointing resulted in a high accuracy measurement of the 3-25 keV X-ray flux and photon index with an accuracy which was only limited by systematic effects. The curvature of the X-ray spectrum could be assessed for a couple of pointings with relatively high X-ray fluxes and long integration times. On three days (April 7, 13th, and 16) the source was also scrutinized with the BeppoSAX X-ray telescopes, revealing the X-ray energy spectrum of the source over the broad energy range from 0.1 keV to  $\sim 200$  keV (Pian et al. 1998).

In Paper I we studied the correlation of the X-ray fluxes with the TeV Gamma-ray fluxes as measured with

the HEGRA Cherenkov telescope system (Aharonian et al. 1999a). For the present study we complemented the data set with the TeV Gamma-ray observations performed with the HEGRA CT1 (Aharonian et al. 1999c), Whipple (Quinn et al. 1999), and CAT (Djannati-Atai et al. 1999) instruments. In Paper I we found a very tight correlation between the 25 keV and 2 TeV fluxes. The flux variability amplitude was approximately 3 times larger at TeV than at X-ray energies, being consistent with a quadratic relationship. An updated version of the X-ray/TeV Gamma-ray flux correlation is shown in Fig. 1. The additional X-ray/TeV Gamma-ray flux pairs confirm the previous finding of a clear flux correlation. However, the quality of the correlation still does not allow us to differentiate between a quadratic X-ray/TeV Gamma-ray relationship and a linear one with a non-zero X-ray flux offset.

The X-ray as well as TeV Gamma-ray data are plagued by systematic errors. In the case of the BeppoSAX data the spectral index below 1 keV is not well determined due to uncertainties in the neutral hydrogen column density. Above 50 keV the scatter of the data points increases more than the statistical errors, indicating systematic uncertainties in the detector response and/or the background subtraction procedure. Some TeV Gamma-ray points taken at approximately the same time with different experiments deviate by more than  $3\sigma$  statistical error from each other, indicative either for very fast source variability, or, for errors on flux-values due to changing atmospheric conditions. While the majority of nearly coincident measurements shows good agreement between different TeV telescopes, the occurrence of some exceptions makes it difficult to decide between models if their predictions differ only for one or two days for which only a single TeV instrument took data. This caveat will be discussed further below, when we compare the models with the data.

The spectral variability at TeV energies has been a matter of debate: the HEGRA group did not detect spectral changes with an accuracy (1-5 TeV photon index) of  $\sim 0.2$  and 0.05 for diurnal and flux selected mean energy spectra, respectively. The CAT group reported the statistically significant detection of a hardness intensity correlation based on the  $F(> 900 \text{ GeV})/F(> 450 \text{ GeV})$  hardness ratio, corresponding to a  $\simeq 0.25$  change in photon index. The two data sets overlapped only partially in time: the HEGRA group did i.e. not take data on April 16, 1997, which is the most important day in the CAT analysis. Konopelko et al. (1999) noted that the stability of the TeV energy spectra, evident in the HEGRA data, can be used to constrain the jet parameters and the intensity of the DEBRA. In the plots shown below, we cross-calibrated the BeppoSAX data relative to RXTE measurements taken at approximately the same time.

Compared to the results shown by Pian et al. (1998) we reduce the BeppoSAX PCA normalizations by up to 35% which eliminates the discontinuity of the BeppoSAX spectra at  $\simeq 15 \text{ keV}$  and is then consistent with the spectral shapes simultaneously measured from 3 keV to 25 keV with RXTE. We also cross-calibrated the CAT, HEGRA CT1, and Whipple Gamma-ray fluxes relative to the ones measured by the HEGRA CT System. Although we obtained a list of CAT fluxes as function of the integer MJDs of the observations, the fractional MJDs of the CAT observations are not known

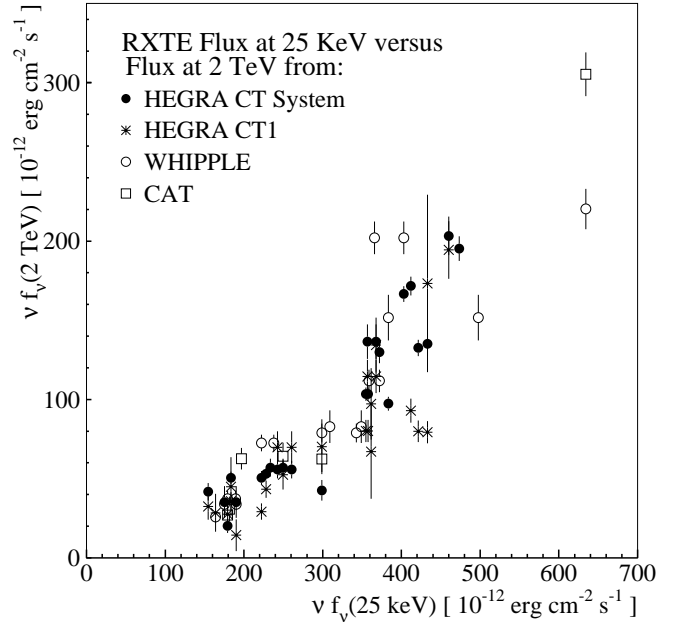


**Figure 1.** Correlation between X-ray (RXTE) and TeV Gamma-ray fluxes. The Gamma-ray fluxes are from CAT (squares), HEGRA CT System (solid points), HEGRA CT 1 (asterisks), and Whipple (open circles). Only observation pairs with less than 6 hrs time delay have been used.

to us. In the following we centered the CAT observations at 12 am UTC.

### 3 MODELING

#### 3.1 Time Dependent SSC Code

The SSC code (Coppi & Blandford 1990; Coppi 1992) assumes a spherical emission region of radius  $R$  which is filled with an isotropic electron population and a randomly oriented magnetic field  $B$  and which approaches the observer relativistically. The motion of the jet towards the observer can be characterized with the jet Doppler factor, defined by

$$\delta_j^{-1} = \Gamma(1 - \beta \cos(\theta)), \quad (1)$$

with  $\Gamma$  the bulk Lorentz factor of the emission plasma, and  $\beta$  the bulk velocity in units of the speed of light of the emitting volume, respectively, and  $\theta$  is the angle between jet axis and the line of sight as measured in the observer frame. The TeV Gamma-ray flux variability on time scale  $\Delta T_{\text{obs}} \approx 12 \text{ hr}$  (Aharonian et al. 1999a) together with causality arguments set an upper limit on the radius of the emission volume:

$$R \lesssim \delta_j c \Delta T_{\text{obs}} \quad (2)$$

However, if the jet moves along a curved path more rapid flares could result from a change of the effective Doppler factor as the jet's radiation beam sweeps across the observer.

The kinetic equations, discretized in energy, take fully into account the non-continuous character of IC processes in the Klein-Nishina regime, and are evolved in time with a two step implicit scheme treating first the photon distribution and subsequently the electron distribution. The length of time steps is chosen such that the number of photons and

particles per energy bin changes per step by less than 20%. The kinetic equation for the photon density (per unit volume and energy)  $n_\gamma$  reads:

$$\frac{\partial n_\gamma}{\partial t} = q_\gamma - p_\gamma - \frac{c}{R(1+\kappa)} n_\gamma \quad (3)$$

where  $q_\gamma d\epsilon$  and  $p_\gamma d\epsilon$  are the rate of photons being produced into and out of the energy interval  $[\epsilon, \epsilon + d\epsilon]$  due to electron-magnetic field, electron-photon and 2-photon interactions. The last term of the right hand side represents photons which escape from the emission region. The factor  $cR^{-1}$  in the last term assures that the photon density approaches steady state values only with a rise/decay constant longer than the light crossing time. The factor  $(1+\kappa(\gamma))$  parameterizes the modification of the photon escape time by Compton processes (Coppi 1992); however, for all the models discussed in the following, we have always  $\kappa \ll 1$ .

The kinetic equation of the electron (and possibly positron) density  $n_e$  reads:

$$\frac{\partial n_e}{\partial t} = Q_e - \frac{\partial}{\partial \gamma} [\dot{\gamma}_{\text{cont}} n_e] + q_e - p_e - \frac{n_e}{t_{e,\text{esc}}} \quad (4)$$

with  $Q_e(\gamma, t)$  from Eq. (5),  $\dot{\gamma}_{\text{cont}}$  gives the decrease of an electron's Lorentz factor per unit time due to continuous energy losses, and  $q_e d\gamma$  and  $p_e d\gamma$  are the rate of particles being produced or scattered into and out of the Lorentz factor interval  $[\gamma, \gamma + d\gamma]$  due to non-continuous energy loss processes, respectively. The last term of the right hand side represents an energy independent escape probability of electrons from the emission region.

The discussion of this paper is limited to the description of the time variable emission components by a one-zone SSC model. A one-zone model is able to approximate multi-zone models as long as the spatial gradients of the magnetic field and the non-linear components in the properly modified kinetic equations (3) and (4) are small. Our code can i.e. mimick “linear inhomogeneous models” as discussed by Kirk, Rieger & Mastichiadis (1998) and Chiaberge & Ghisellini (1999). While EC models can be dominantly linear, the SSC model is inherently strongly non-linear: the synchrotron component directly follows the evolution of the electron population, but the IC component results from the interaction of the electron population with the self-produced synchrotron photons. Since electrons and synchrotron photons traverse the emission region on a time scale of  $R/c$ , one expects that the IC component lags the synchrotron component by approximately one light crossing time (Coppi & Aharonian 1999). This is the most drastic time lag effect expected in the SSC model. To first order approximation our code takes the non-vanishing source extension into account through the last term in Eq. 3. As a consequence, the code is able to describe flux variations even on time scales of order  $R/c$  in a qualitatively correct way. We think that this approximate treatment of light crossing time effects is fully justified for modeling the 1997 Mrk 501 observations as the available data do not indicate that the geometry of the emitting plasma blob decisively influences the temporal evolution of the X-ray and TeV Gamma-ray fluxes: no evidence for a non-zero time lag between the synchrotron and IC radiation components has yet been found, the upper limit being about 12 hrs (Aharonian et al. 1999a; Aharonian et al. 1999c; Paper I; Sambruna et al. 2000).

We fit the full two months data train using a single emission volume. As we will point out in the discussion, it might be that individual flares (of durations on the order of  $\sim 1$  day) are produced by independent emission regions. Upon flaring, a region would expand adiabatically, and thus fade away quickly. Even in this case, our model should give reasonable results for two reasons: (i) as it turns out the best fitting models have particle escape times on the order of the flux variability time scale; (ii) the tight X-ray/TeV Gamma-ray flux correlation argues for a very similar size of the emission regions. As a consequence of the first fact, each flare is produced by freshly accelerated electron populations and modeling the flares with one emission region gives similar results as using several disjunct emission regions.

### 3.2 Treatment of Particle Acceleration

Given the sparse observational sampling of the data set which we study in this paper in time and wavelength, we did not embark on modeling the acceleration process in detail but used instead an “external” acceleration function. We parameterize the production rate of freshly accelerated particles as function of electron Lorentz factor  $\gamma$ , spectral index of particle acceleration  $p$ , normalization  $Q_0(t)$ , minimum Lorentz factor  $\gamma_{\text{min}}$ , and high energy cut-off  $\gamma_{\text{max}}(t)$  as follows:

$$Q_e(\gamma, t) = Q_0(t) \gamma^{-p} \exp(-\gamma/\gamma_{\text{max}}(t)) \Theta(\gamma - \gamma_{\text{min}}) \quad (5)$$

with  $\Theta(x) = 0$  for  $x < 0$  and  $\Theta(x) = 1$  for  $x \geq 0$ . We use the canonical value of  $p = 2$  expected for diffusive particle acceleration at strong shocks (Bell 1978; Blandford & Ostriker 1978) and do not consider the ramifications arising from the non-linear modification of the shock structure due to the backreaction of accelerated particles (Bell 1987) and mildly or ultra-relativistic shock velocities (see the recent review by Kirk & Duffy 1999; Kirk et al. 2000; Achterberg 2001).

The low-energy cutoff in the spectrum of accelerated electrons  $\gamma_{\text{min}}$  is a critical model parameter. If the radiative cooling time of electrons with Lorentz factor  $\gamma_{\text{min}}$  is shorter than all the other characteristic time scales of the system, the main break of the electron spectrum occurs at  $\gamma_{\text{min}}$ . Thus, at high enough values ( $\sim 10^5$ ),  $\gamma_{\text{min}}$  determines the energies at which the synchrotron and IC SEDs peak. On theoretical grounds one expects much lower values of between 1 and the proton to electron mass ratio  $m_p/m_e = 1836$  (Hoshino et al. 1992; Levinson 1996; McClements 1997). We will use in the following a relatively low value of  $\gamma_{\text{min}} = 1000$  as the fiducial value and will discuss higher values at several points.

We characterize the acceleration luminosity  $L_e$  by the pair-compactness parameter (Coppi 1992):

$$l_e = \frac{L_e \sigma_T}{R m_e c^3} = \frac{8\pi R^2 \sigma_T}{3c} \int \gamma_e Q(\gamma_e) d\gamma_e \quad (6)$$

### 3.3 Treatment of Extragalactic Extinction

The TeV Gamma-ray spectra are expected to be modified by extragalactic extinction due to pair production processes of the TeV Gamma-rays with photons of the DEBRA. The

uncertain DEBRA intensity in the relevant 0.5-30 $\mu$ m wavelength range introduces a major uncertainty in the modeling of the source. While earlier estimates of the DEBRA level predicted negligible extinction at Gamma-ray energies below  $\sim 1$  TeV, more recent observational and theoretical efforts suggest that this might not be true (Primack et al. 2001). We think that model estimates of the DEBRA still have not reached the reliability that we should limit our computations to a specific DEBRA model. Rather we will treat the modification of the TeV flux level and energy spectrum as not fully constrained. Clearly, the DEBRA extinction does not modify the relative TeV Gamma-ray flux variations and we use the information encoded in the relative flux changes by fitting the TeV Gamma-ray fluxes subject to a common constant scaling factor  $\xi$ . At 2 TeV one expects a  $\xi$ -value of between 0.2 and 1. We have varied the  $\xi$ -values in this range, and the qualitative conclusions presented below are robust and do not depend on the exact value of  $\xi$ . For the detailed fits presented below, we will take  $\xi \simeq 0.5$ , a value which seems to be preferred by recent observations and theoretical modeling.

Due to rather large statistical errors on diurnal Gamma-ray photon indices we did not attempt to fit the variations of the spectral hardness with the SSC code. We did check if the TeV Gamma-ray energy spectra of our best-fit SSC model, modified by the extinction predicted by our favored DEBRA model, is consistent with the observed one.

### 3.4 Fitting Procedure

The free parameters of our model are the radius of the emission volume  $R$ , the jet Doppler factor  $\delta_j$ , the mean magnetic field  $B$ , the escape time of relativistic electrons from the emission region  $t_{\text{esc}}$ , the normalization of the electron acceleration rate  $Q_0$ , and the minimum and maximum Lorentz factors of accelerated particles  $\gamma_{\text{min}}$  and  $\gamma_{\text{max}}$ . We fit the April and May, 1997 RXTE 10 keV fluxes and 3-25 keV photon indices and the 2 TeV fluxes derived from CAT, HEGRA, and Whipple measurements. Given a hypothesis of what causes the flaring activity (a variable  $Q_0(t)$ ,  $\gamma_{\text{max}}(t)$ , and/or  $\delta_j(t)$ ) we fit the data in 2 steps:

(i) For a set of parameters ( $R$ ,  $\bar{\delta}_j$ ,  $B$ ,  $\gamma_{\text{min}}$ ,  $t_{\text{esc}}$ ) we determine the simplest possible function  $Q_0(t)$  and  $\gamma_{\text{max}}(t)$ , or for some models  $\delta_j(t)$ , which fit the X-ray flux amplitudes. Hereby, “the simplest possible functions” means that given the X-ray flux measurements at times  $t_i$  (in the jet frame) we use simple prescriptions to determine  $Q_0$ ,  $\gamma_{\text{max}}$ , or  $\delta_j$  at the times  $t'_i = t_i - \Delta t$ , and compute intermediate values by simple interpolation. The parameter  $\Delta t$  is the time by which the photon density in the emission region reacts to changes of the electron spectrum. In general, the optimal delay  $\Delta t$  depends on the time scale on which electrons cool and escape from the emission region. Due to the constraints on the time lag between low (3 keV) and high energy X-rays (30 keV) to be smaller than  $\sim 10$  hrs (Paper I), the delay of all our models is dominated by the light crossing time and the treatment of Eq. (3) results in an optimal value of  $\Delta t \simeq 2.5 R c^{-1}$ . For variations of  $\delta_j$  we use  $\Delta t = 0$  for obvious reasons.

We determine the values  $Q_0(t_i)$ ,  $\gamma_{\text{max}}(t_i)$ , and  $\delta_j(t_i)$  iteratively by making a first guess, computing the SSC model,

and adjusting the values until the X-ray fluxes are described satisfactorily. Usually, between 2 and 5 iterations are needed. The reader should keep in mind that the true time history of the acceleration process could be more complex.

(ii) We vary the parameters ( $R$ ,  $\bar{\delta}_j$ ,  $B$ ,  $\delta_j$ ,  $t_{\text{esc}}$ ) to obtain the best fit to the observed X-ray photon indices and TeV Gamma-ray flux amplitudes. The quality of the fits is characterized by  $\chi^2$ -values, computed for the X-ray photon indices and for the TeV Gamma-ray fluxes. We exclude the first 2 days of each observation period from entering the  $\chi^2$ -values, since the results strongly depend on the unknown behavior of the source before the observations commenced. Note that the reduced  $\chi^2$ -values of the X-ray fluxes and photon indices and of the TeV Gamma-ray fluxes exceed 1 by a wide margin, showing that the experimental statistical errors are smaller than the accuracy of our models and/or that the experimental systematic errors (often only poorly determined) are non-negligible.

Computing the  $\chi^2$ -values, we scale all TeV Gamma-ray fluxes by a common factor  $\xi$  with  $0.2 < \xi < 1$ . For each model we state the  $\xi$ -value which we used as well as  $\eta$ , the implied amount of steepening of the 1-5 TeV energy spectrum. Due to the strong dependence of the IC luminosity on the radius of the emission volume, the modeling does not give any constraints on  $\xi$ . As will be discussed in Sect. 5, the uncertainty in the SSC model parameters do not allow us to constrain  $\eta$  either.

After obtaining in this way the best fits we test the predicted SEDs (Spectral Energy Distributions) for consistency with the broadband X-ray spectra from the BeppoSAX observations, and an MeV upper limit from EGRET (Catanese et al. 1997). We do not fit the TeV photon indices, since the typical errors are larger than the predicted variations. We do check if the modeled photon indices are in accord with the results from CAT and HEGRA observations. Furthermore models which produce steeper than observed TeV energy spectra are rejected since all current DEBRA models predict to steepen the TeV energy spectra.

## 4 RESULTS OF THE TIME DEPENDENT MODELING

SSC Blazar models have extensively been discussed in the literature. The models can roughly be classified according to 2 criteria (see Table 1):

(i) According to what produces the observed Gamma-ray flares: basically, almost every parameter of the SSC model has been invoked by at least one group to account for the Blazar flaring activity.

(ii) According to the mechanism that determines the energies at which the synchrotron and IC SEDs peak. The SED peak energies are either determined by the minimum Lorentz factor  $\gamma_{\text{min}}$  of accelerated particles, or, by the balance between radiative cooling times and the shorter of particle escape time and the characteristic duration of individual flares (sometimes referred to as injection time scale, or, dynamical time scale of the jet).

The modeling of the full data train is computationally very intensive and we therefore focused on exploring only the models which seemed most promising to us. While the time

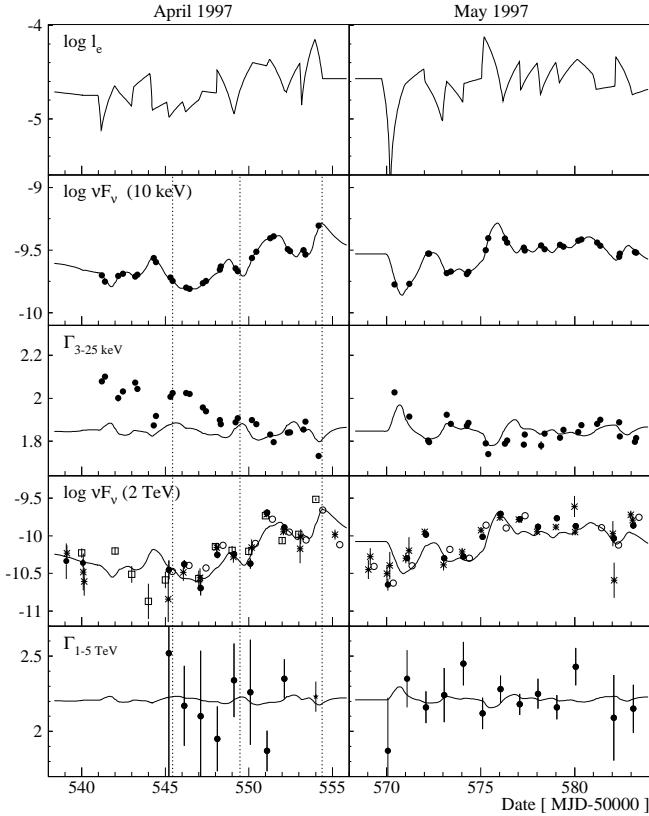


**Figure 2.** X-ray and TeV Gamma-ray data (data points) from April, 1997 (left column) and May, 1997 (right column) with SSC model fit (lines). Here, model flares are caused by a time dependent  $Q_0(t)$ . The panels show from top to bottom: (i) the logarithm of the injection compactness  $l_e$ , (ii) the logarithm of the 10 keV X-ray energy flux ( $10^{-12}$  erg  $\text{cm}^{-2}$   $\text{s}^{-1}$ ), (iii) the X-ray 3-25 keV photon index, (iv) the logarithm of the 2 TeV energy flux ( $10^{-12}$  erg  $\text{cm}^{-2}$   $\text{s}^{-1}$ ), and (v) the 1-5 TeV photon index. The Gamma-ray fluxes are from CAT (squares), HEGRA CT System (solid points), HEGRA CT 1 (asterisks), and Whipple (open circles). TeV photon indices have only been published by the HEGRA group. The value for April 16 has been inferred from the energy spectrum published by Djannati-Atai et al. (1999). The vertical dashed lines show the days with BeppoSAX observations (April 7, 11, and 16) which will be discussed in more detail further below. The model parameters are:  $\delta_j = 45$ ,  $R = 1.1 \times 10^{16}$  cm,  $B = 0.014$  G,  $t_{\text{esc}} = 10 R c^{-1}$ ,  $\gamma_{\text{min}} = 10^3$ ,  $\gamma_{\text{max}} = 2.5 \times 10^7$ ,  $\xi = 0.5$ ,  $\eta = 0.2$ .

resolved analysis clearly rules out some models, it gives fits of very similar quality for others. Our difficulties to distinguish between models mainly derive from two facts:

- (i) From the limitations of the data set, namely sparse observational sampling in time and energy, and systematic errors on X-ray energy spectra and TeV Gamma-ray fluxes.
- (ii) From the unknown modification of the TeV Gamma-ray energy spectra by extragalactic extinction.

Keeping these limitations in mind, we discuss the fit results with a focus on pointing out which models are capable of correctly describing the qualitative behavior of the X-ray and TeV Gamma-ray radiation. Table 2 lists the model parameters of the SSC models shown in the figures.

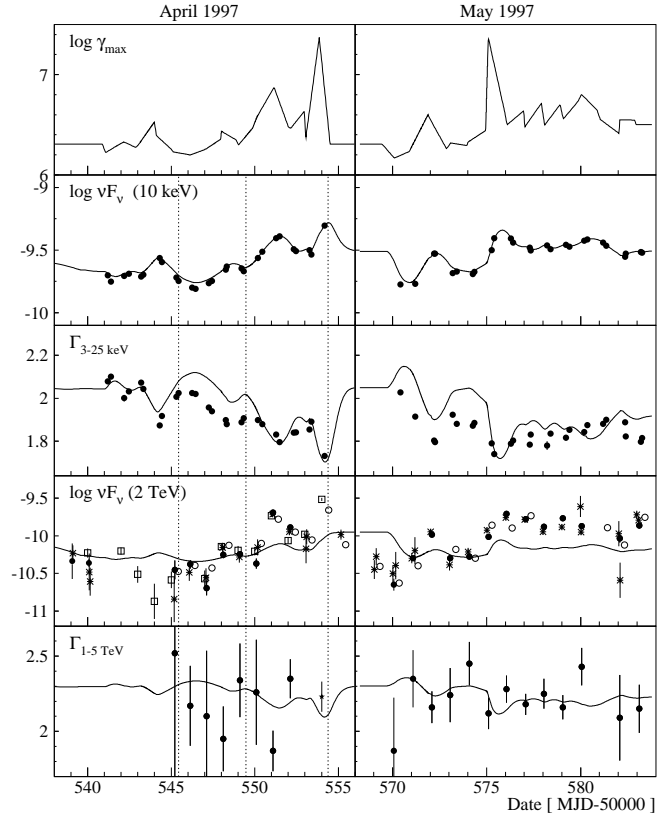


**Figure 3.** Same as in Fig. 2, but with flaring activity through a time dependent maximum Lorentz factor of accelerated particles  $\gamma_{\text{max}}(t)$ . The upper panel shows here  $\gamma_{\text{max}}(t)$ . The model parameters are:  $\delta_j = 45$ ,  $R = 1.5 \times 10^{16}$  cm,  $B = 0.009$  G,  $t_{\text{esc}} = 3 R c^{-1}$ ,  $\gamma_{\text{min}} = 10^3$ ,  $\xi = 0.5$ ,  $\eta = 0.2$ .

## 4.1 One-Component Models

### 4.1.1 Time variability through $Q_0(t)$

We first consider time variability through a varying rate of accelerated particles. If  $Q_0(t)$  varies, the SSC mechanism automatically produces a more than linear increase of TeV flux as function of X-ray flux. Fig. 2 shows the observed and modeled X-ray and Gamma-ray flux amplitudes and photon indices. Whenever the size of the emission region satisfies Eq. (2), and either rapid particle losses ( $t_{\text{esc}}$  not much larger than  $R c^{-1}$ ) or a sufficiently large magnetic field allow flares to decay rapidly enough, the X-ray amplitude can be described to arbitrary precision. This also applies for all the models described in the following. Thus, we subsequently focus on the X-ray photon indices and the TeV Gamma-ray fluxes for measuring the quality of a fit.

Although the model describes the TeV flux levels, it fails to reproduce the range of observed X-ray photon indices. The stability of the X-ray spectrum is a solid property of this model. The spectral variability shown in Fig. 2 is already the result of a fine tuning between the parameters  $B$ ,  $t_{\text{esc}}$ , and  $\gamma_{\text{max}}$ . Most realizations of this model result in substantially less spectral variability. For the model parameters of Fig. 2 the location of the break in the synchrotron SED is given by the competition of the escape of electrons on time scale  $t_{\text{esc}}$  and their radiative cooling through synchrotron and IC emission on time scale  $t_{\text{rad}}$ . High energy electrons with  $t_{\text{rad}} \lesssim$

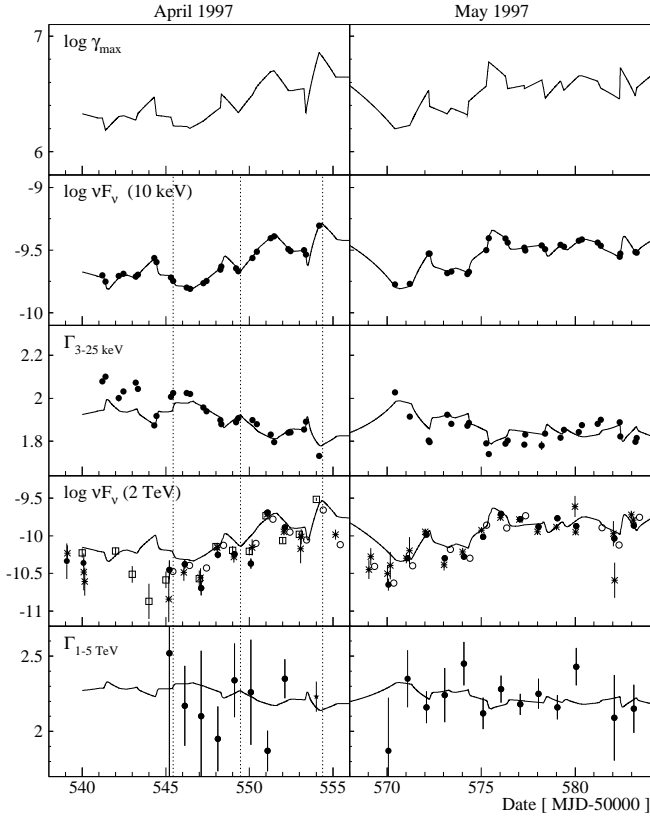


**Figure 4.** Same as in Fig. 3, but with flaring activity through time dependent  $Q_0(t)$  and  $\gamma_{\max}(t)$  with  $\gamma_{\max} \propto Q_0^2$ . The upper panel shows here  $Q_0(t)$ . The model parameters are:  $\delta_j = 45$ ,  $R = 3.2 \times 10^{15}$  cm,  $B = 0.035$  G,  $t_{\text{esc}} = 3 R c^{-1}$ ,  $\gamma_{\min} = 10^3$ ,  $\xi = 0.5$ ,  $\eta = 0.1$ .

$R c^{-1}$  cool almost instantly. Low energy electrons with  $t_{\text{rad}} \gtrsim t_{\text{esc}}$  do not have time to cool before they escape the emission region. The result is that the spectrum does only vary over a rather small region where  $t_{\text{rad}} \sim t_{\text{esc}}$ . The smearing of the break in the electron spectrum due to the width of the synchrotron emissivity results in a rather stable break of the synchrotron spectrum. Qualitatively we see a similar behavior also for larger values of  $t_{\text{esc}}$ . The reason is that the rise and decay times of the flares are of the same order of magnitude as the time between flares. Thus, all observed electron energy spectra radiatively cool to approximately the same degree with a break at approximately the same Lorentz factor.

Inspection of the fitted and observed TeV fluxes shows a strong discrepancy at MJD 50544. A TeV data point that suggests a very low flux is bracketed by X-ray observations of relatively high fluxes. This model as well as the models described below fail to describe this exceptional anticorrelation. The low TeV flux may either be indicative of a short period of low X-ray and TeV Gamma-ray activity between the two X-ray observations, or of an underestimated TeV flux due to instrumental or atmospheric irregularities. Note how little the TeV photon index changes in this model.

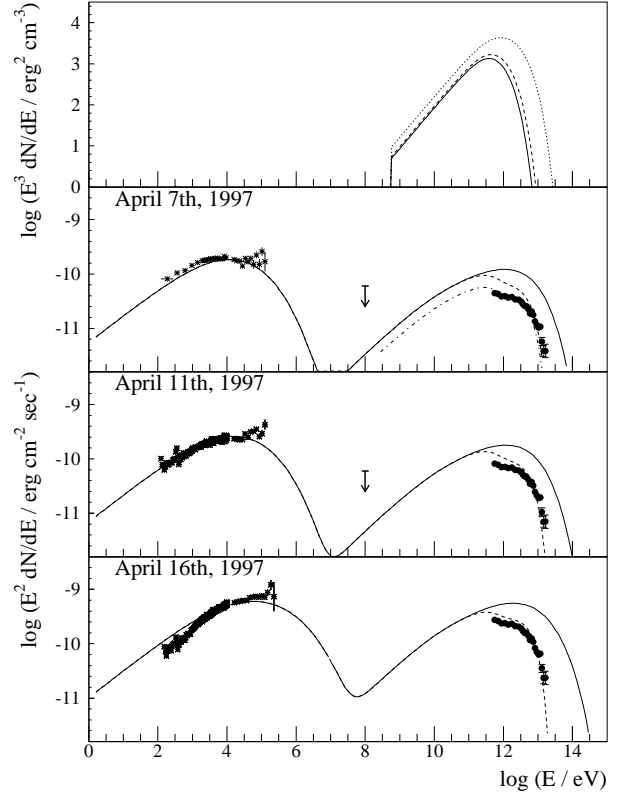


**Figure 5.** For the model of Fig. 4 the upper panel shows the electron energy spectra ( $E^3 dN/dE$ , energy  $E$  in the jet frame) responsible for the observations of April 7 (solid line), April 11 (dashed line) and April 16 (dotted line). The lower three panels compare the observed (points) with the modeled (solid line) SEDs (energy in observer’s frame). For illustrative purposes the dashed line shows the TeV Gamma-ray energy spectra modified by extragalactic absorption as predicted by the DEBRA model “LCDM, Salpeter Stellar Initial Mass Function” of Primack et al. (2001). For April 7 the dashed-dotted line shows the same absorbed Gamma-ray spectrum, but normalized to the TeV flux at 2 TeV to facilitate comparison of the spectral shapes. Asterisks show the BeppoSAX data normalized to the flux measured with RXTE. The solid points show the shape of the HEGRA 1997 time averaged Mrk 501 energy spectrum (Aharonian et al. 1999b; Aharonian et al. 2001b). The  $2\sigma$  upper limit at 100 MeV has been derived from EGRET observations between April 9th and April 15th, 1997 under the assumption of a constant emission level (Catanese et al. 1997).

#### 4.1.2 Time variability through $\gamma_{\max}(t)$

As a second model we tested flares caused exclusively by a variation of the high energy cutoff  $\gamma_{\max}$  of accelerated particles. While  $\gamma_{\max}$  may depend on the details of the magnetic field structure in the surrounding of a particle accelerating shock, other parameters influencing mainly the acceleration of lower energy electrons could remain constant. Historically, such models were motivated by observation of the Blazar Mrk 421 which showed dramatic X-ray and TeV Gamma-ray flux variability accompanied by only minor optical flux variability.

Varying  $\gamma_{\max}$  alone we did not achieve a satisfactory fit to the data. A typical result is shown in Fig. 3. As before the

X-ray fluxes can be described to arbitrary precision. While the model has no difficulty in producing the observed range of X-ray photon indices, it fails to describe the X-Ray / TeV Gamma-ray flux correlation: the predicted TeV Gamma-ray fluxes hardly vary at all. Combinations of Doppler factor and magnetic field where the TeV flux changes more strongly than the X-ray flux result in steeper than observed TeV energy spectra. The time variation of  $\gamma_{\max}$  causes large flux and spectral variability only at energies  $\gg 10$  TeV where the inherent TeV energy spectrum is extremely soft (photon index  $\gtrsim 2.5$ ). Extragalactic extinction can not remedy this shortcoming since it is believed to steepen and not to soften the TeV energy spectra.

Tavecchio et al. (2001) studied parametric SSC model fits to Mrk 501 snapshot data and concluded that the maximum Lorentz factor of accelerated particles is mainly responsible for the flaring activity. However, detailed inspection of their fit parameters shows that they described the data by varying the break of the electron spectrum rather than the high energy cutoff. Furthermore, the fits involve a substantial variation of the normalization of the electron spectrum (i.e. the acceleration rate).

#### 4.1.3 Time variability through $Q_0(t)$ and $\gamma_{\max}(t)$

Models in which both,  $Q_0$  and  $\gamma_{\max}$ , change with time have been invoked to account for the secular changes of the Mrk 501 X-ray (Pian et al. 1998; Sambruna et al. 2000) and TeV Gamma-ray (Aharonian et al. 2001a) energy spectra. In models of diffusive electron acceleration at strong shocks the electron acceleration rate  $Q_0$  is determined by the rate with which particles are “injected” into the acceleration process. The high energy cutoff of accelerated electrons  $\gamma_{\max}$  is determined by the competition between electron energy gains and energy losses. Changing plasma properties most probably affects both, the injection rate and the high energy cutoff. Due to the uncertain nature of the particle injection mechanism we choose a simple parametric description to describe the correlation between  $Q_0$  and  $\gamma_{\max}$ :

$$\gamma_{\max} = Q_0^\alpha \quad (7)$$

and treat the exponent  $\alpha$  as an additional free parameter of the fit. The  $\chi^2$ -value of the X-ray photon indices show a pronounced minimum for a value of  $\alpha = 2$ , and Fig. 4 shows a SSC fit to the data. The model describes the RXTE and Gamma-ray data rather satisfactorily. As mentioned above, the Gamma-ray flux discrepancy at MJD 50544 might be explained by a too naive estimation of the source activity from the RXTE data with relatively sparse observational sampling.

During the first 3 days of the April campaign the model X-ray indices are by  $\sim 0.1$  harder than the observed ones, a discrepancy which is shared also by all subsequent models. Compared to other days of similar X-ray flux levels, the X-ray spectrum of the first three days with RXTE coverage was very soft, indicating that the source properties did evolve during the 2 months campaign.

Although only 3 BeppoSAX observations were performed during 1997, the data is very constraining since it covers the broad energy range from 0.1 keV to  $\sim 200$  keV. The long BeppoSAX pointings of  $\simeq 12$  hrs duration bracketed the RXTE and TeV Gamma-ray observations. The

comparison of the modeled and observed broadband energy spectra is shown in Fig. 5. For April 7 and 11 the model X-ray spectra are softer than the observed ones at and above  $\sim 50$  keV. For April 16, the overall X-ray energy spectrum is too soft. The hard observed energy spectra above 50 keV indicate that the high energy cutoff of accelerated particles is not the reason for the observed spectral variability: for all three days the true energy spectra probably cut off at energies well above 200 keV. In the next section we will present models which give also a harder X-ray energy spectrum for April 16.

In Fig. 5 also the modeled and observed TeV energy spectra are shown. We used for all three days the time averaged 1997 HEGRA TeV Gamma-ray energy spectrum normalized at 2 TeV to the mean flux measured on that day with all operational TeV telescopes. The use of the time averaged energy spectrum is justified by the fact that all the HEGRA data taken during 1997 are consistent with the shape of the time averaged energy spectrum (see however Djannati-Atai et al. (1999)). For illustrative purposes the dashed lines in Fig. 5 show the predicted TeV Gamma-ray energy spectra modified by extragalactic absorption, computed for the DEBRA model “ $\Lambda$ CDM, Salpeter Stellar Initial Mass Function” of Primack et al. (2001). For April 7, the model under-predicts the TeV flux, and the dashed-dotted line shows a properly normalized model to facilitate the comparison of the shape of modeled and observed energy spectrum. We will further discuss the agreement between observed and modeled SEDs below for the models which give a better overall fit to the X-ray data.

## 4.2 Two-Component Models

The region near the presumed central black hole as well as various regions along the jet might emit X-rays in Bremsstrahlung, IC, or Synchrotron processes without producing a comparable luminosity at Gamma-rays (see also Błażejowski et al. (2000), Bicknell, Wagner & Groves (2001)). Thus it is conceivable, even probable, that the X-ray emission from Mrk 501 is “contaminated” by an emission component which varies on longer time scales than the TeV Gamma-ray radiation. While all the one-component models described in the previous section failed to fully describe the data, we find that the addition of a quasi-stationary X-ray component substantially improves the situation. Varying contributions of the quasi-stationary soft and the time variable hard component are able to account for the large spectral changes observed at X-rays.

Over the narrow spectral range from 3 keV to 25 keV we describe the quasi-steady X-ray component by a power law. We determined possible values of flux level and spectral slope of the quasi-stationary component from extrapolating the 10 keV vs. 2 TeV flux correlation towards zero Gamma-ray flux, and the 10 keV flux vs. 3-25 keV photon index correlation (Paper I) towards zero X-ray flux, respectively. Due to the scatter of both correlations this criterion gave a range of allowed values. We chose the values which resulted in the the best two-component SSC fits to the data, namely a 10 keV amplitude  $\nu F_\nu = 10^{-10}$  erg cm $^{-2}$  s $^{-1}$  and a photon index of 2.2.

In the following we describe different incarnations of two-component models: two with variability through a time

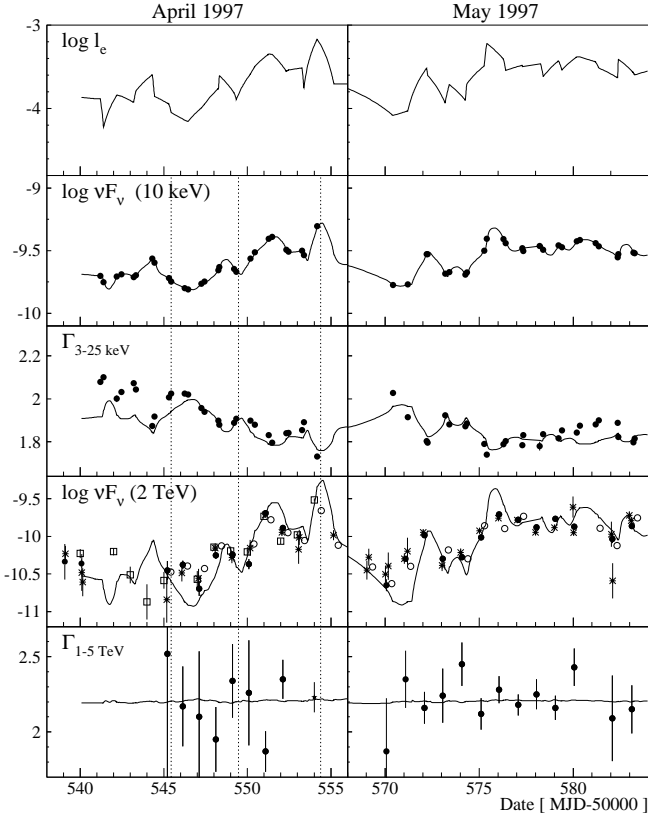


**Figure 6.** Fit of a SSC model with two emission components: (i) a quasi-stationary X-ray component, and, (ii) a time variable X-ray/TeV Gamma-ray component, flares produced through  $Q_0(t)$ . Data and units are the same as in Fig. 2. The model parameters are:  $\delta_j = 45$ ,  $R = 3.4 \times 10^{15}$  cm,  $B = 0.014$  G,  $t_{\text{esc}} = 3 R c^{-1}$ ,  $\gamma_{\text{min}} = 10^3$ ,  $\gamma_{\text{max}} = 2.3 \times 10^7$ ,  $\xi = 0.5$ ,  $\eta = 0.4$ .

dependent rate of accelerated particles, and one with a time dependent Doppler factor of the SSC emission region.

#### 4.2.1 Time variability through $Q_0(t)$ , $\gamma_{\text{min}} = 1000$

First we consider a two-component model with flares caused by varying  $Q_0(t)$ . Since the spectral variability at X-rays is produced by the varying dominance of the soft quasi-static and the hard time dependent components no additional spectral variability has to be produced by a changing  $\gamma_{\text{max}}$  and we use a fixed  $\gamma_{\text{max}}$  corresponding to a high energy cut-off in the synchrotron spectrum at MeV energies. Fig. 6 shows the fit of the two-component model (see figure caption for model parameters). Compared to the one-component  $Q_0(t)$  model shown in Fig. 2, the additional quasi-stationary soft component significantly improves the fit of the X-ray photon indices. The improvement is most pronounced for the April data. The model also describes well the TeV Gamma-ray fluxes, with the notorious exception of MJD 50544.

Finally, we compare the model SEDs with the one measured by BeppoSAX. Based on the data of one of the three BeppoSAX observations (we used the observation of April 11), one can determine the spectrum of the quasi-stationary X-ray component outside the energy range covered by the RXTE observations. The other two observations can then

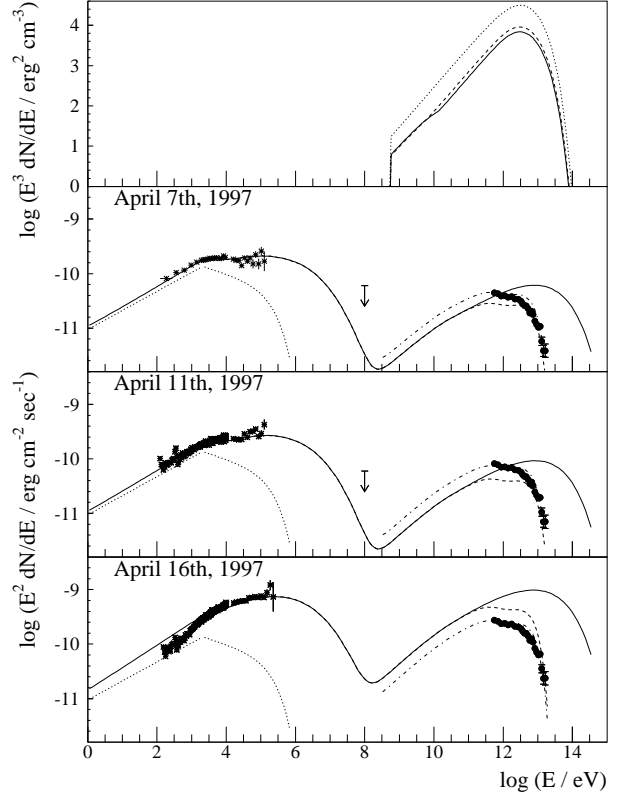


**Figure 7.** Same as in Fig. 5 but for the two-component model with time variable  $Q_{0j}(t)$  shown in Fig. 6. In the lower three panels, the dotted line shows the quasi-stationary X-ray component, and the dashed-dotted lines show the absorbed Gamma-ray energy spectra normalized at 2 TeV to the observed ones.

be used to check the model predictions. The upper panel of Fig. 7 shows the electron energy spectra averaged over the integration time of the 3 BeppoSAX pointings. The lower three panels compare the modeled with the observed SEDs. By construction, the model describes the X-ray data of April 7; the fit to April 11 is also good, but the model spectrum of April 16 is too soft. More detailed inspection shows that the model fails to describe the temporal evolution of the  $\lesssim 1$  keV fluxes, i.e. for April 16 it produces too much flux below 1 keV.

Remarkably, the predicted TeV energy spectrum, modified by extragalactic extinction according to the LSDM model of Primack et al. 2001 fits the HEGRA time averaged spectrum very well.

#### 4.2.2 Time variability through $Q_0(t)$ , $\gamma_{\text{min}} = 10^5$

A similar model with a high value of  $\gamma_{\text{min}} \sim 10^5$  does not show these difficulties. In this case the break in the energy spectrum is more abrupt and the peak of the synchrotron SED of the time variable component is narrower than in the previous case. Viable models with high minimum Lorentz factors are located in a completely different region of parameter space: at Doppler factor 45, we infer a magnetic field of  $B = 1$  G and a radius of  $5 \times 10^{13}$  cm compared to the values of  $B = 0.014$  G and  $R = 3 \times 10^{16}$  cm for the

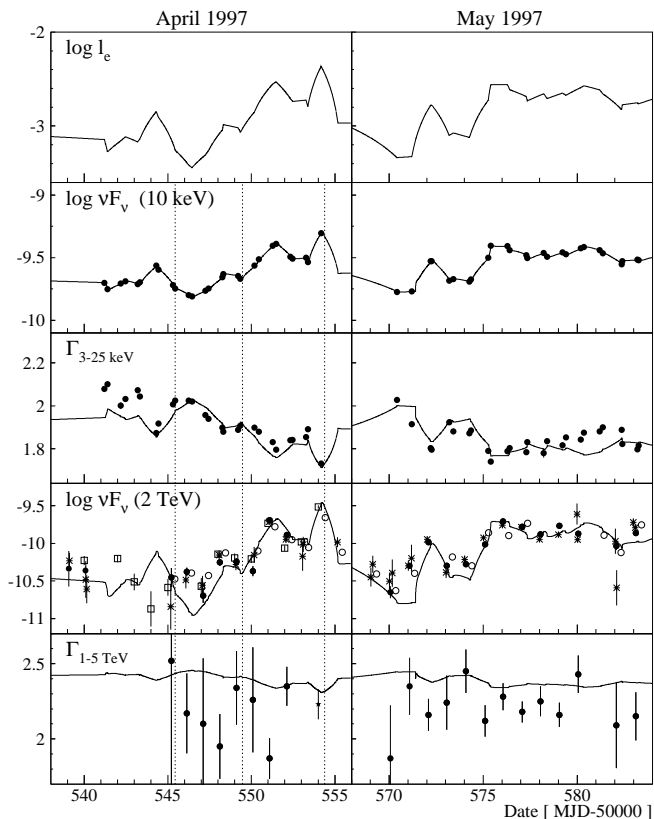


**Figure 8.** Same as in Fig. 6, but for the two-component model with  $\gamma_{\min} = 10^5$ . The model parameters are:  $\delta_j = 45$ ,  $R = 4.5 \times 10^{13}$  cm,  $B = 1.1$  G,  $t_{\text{esc}} = 10^4 R c^{-1}$ ,  $\gamma_{\min} = 10^5$ ,  $\gamma_{\max} = 1.4 \times 10^7$ ,  $\xi = 0.5$ ,  $\eta = 0.00$ .

previous model. A large magnetic field is required to assure sufficiently rapid cooling of electrons with Lorentz factors above  $\gamma_{\min}$  to Lorentz factors below  $\gamma_{\min}$ . The latter electrons are needed to produce the optical and UV seed photons, and partially, also for producing IC Gamma-rays in the 250 GeV to  $\sim 1$  TeV energy range. A small radius  $R$  follows than from the requirement to produce the observed IC luminosity, given the large magnetic field and the “narrow” synchrotron SED.

The best-fit result is shown in Figs. 8 and Figs. 9. It can be recognized that the use of  $\gamma_{\min} = 10^5$  substantially improves the fit to the broadband BeppoSAX data. Even without any extragalactic extinction the model of the TeV Gamma-ray data is very soft and only barely consistent with the observed data below 10 TeV. Only above 10 TeV, the model implies a slight amount of extinction. Note the pronounced break of the IC spectrum at  $\sim 2$  TeV. Obviously, fitting a power law to a small portion of such a spectrum and inferring the DEBRA intensity from the deviation of the observed spectrum from this power law will not produce correct results.

#### 4.2.3 Variability through $\delta_j(t)$ , $\gamma_{\min} = 5 \times 10^5$

In the framework of one-component models, a emitting blob with constant and isotropic emission in its rest frame but with a varying angle between its motion and the line of sight can not account for the 1997 X-ray and TeV Gamma-

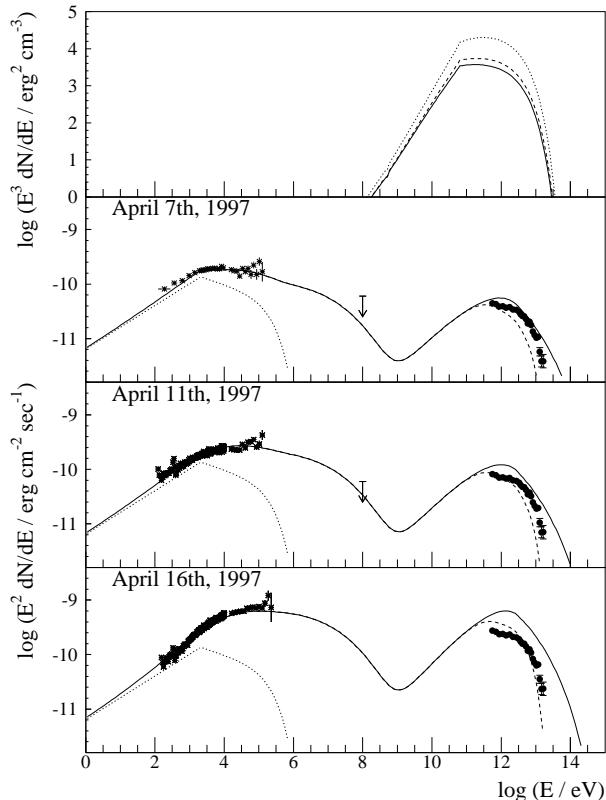


**Figure 9.** Same as in Fig. 7 but for the two-component model with  $\gamma_{\min} = 10^5$ , shown in Fig. 8.

ray flares. The reason is that the large variability of the peak energy of the synchrotron SED would imply a large change of the blob’s Doppler factor and as a consequence a much larger than observed flux variability (Paper I). In a two-component model however, a variable Doppler factor can explain the flux variability: the X-ray energy spectra mainly change due to the relative dominance of the quasi-stationary and the time-variable X-ray components. Figs. 10 and 11 show the two-component fit to the time resolved data and the broadband spectral data, respectively. The model gives an excellent fit to the data.

## 5 DISCUSSION

In this paper we describe the time resolved modeling of the X-Ray and TeV Gamma-ray data of a 2 month observation campaign. The time resolved analysis is plagued by the sparse observational sampling and the unknown modification of the TeV Gamma-ray energy spectrum by extragalactic extinction. However, modeling the X-ray fluxes and energy spectra and the relative changes of the TeV Gamma-ray fluxes and photon indices allows us to exclude some hypothesis about the flare origin. Furthermore, we are able to verify that simple but self-consistently evolved SSC models based on canonical power-law energy spectra of accelerated electrons are able to account for the very detailed observational data. More specifically, our conclusions from the time dependent modeling are as follows:

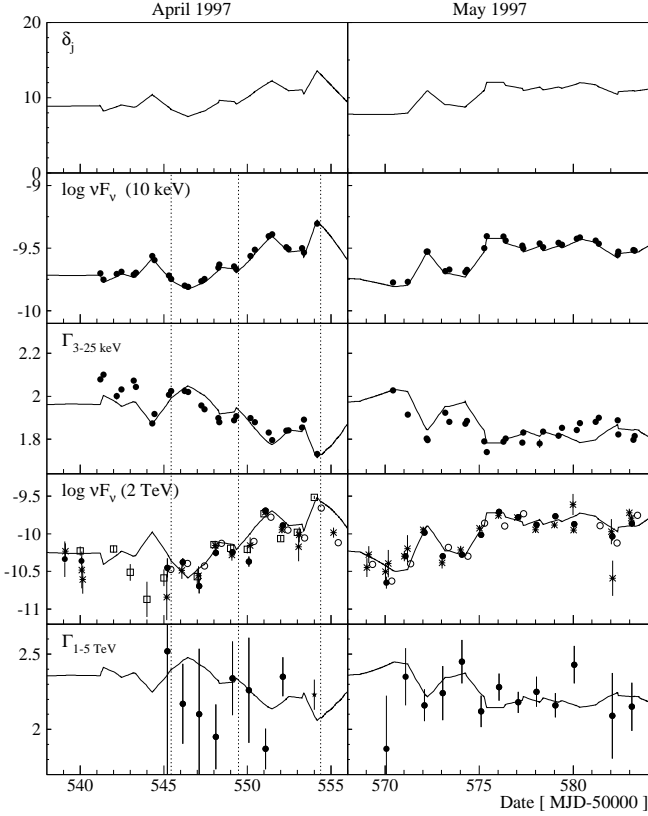


**Figure 10.** Fit of a SSC model with two emission components: (i) a quasi-stationary X-ray component, and, (ii) a time variable X-ray/TeV Gamma-ray component, flares produced through  $\delta_j(t)$ . The upper panel shows here  $\delta_j(t)$ , and the other data and units are the same as in Fig. 2. The model parameters are:  $R = 10^{15}$  cm,  $B = 0.16$  G,  $t_{\text{esc}} = 10 R c^{-1}$ ,  $\gamma_{\text{min}} = 4.5 \times 10^5$ ,  $\gamma_{\text{max}} = 2.9 \times 10^7$ ,  $\xi = 0.5$ ,  $\eta = 0.04$ .

(i) One-component models do not fully describe the data. While, by construction, the models succeed in accounting for the temporal evolution of the X-ray fluxes they do not adequately predict at the same time the range of observed X-ray spectral indices, the broadband 0.1 keV-200 keV energy spectra, and the variation of the TeV Gamma-ray fluxes. I.e. models in which only the rate of accelerated particles or only the maximum Lorentz factor of accelerated particles produce the flaring activity do not work.

(ii) Two-component models give surprisingly good fits to the data. In these models, the X-rays originate from a superposition of a soft quasi-steady component and a hard rapidly variable component. We found two models which give an excellent fit: in the first model flares are produced by a time dependent rate of accelerated particles. In the second model, a changing Doppler factor causes the flares. In both models, changes of the observed X-ray energy spectrum mainly result from the relative dominance of the quasi-stationary and the time-variable X-ray component.

(iii) Accurate fits to the BeppoSAX broadband data require a large minimum Lorentz factor of accelerated particles on the order of  $\gamma_{\text{min}} = 10^5$ .

(iv) Degeneracy in both, model variant and jet parameters, prevents us to use the time resolved SSC calculations to substantially tighten the constraints on the amount of TeV

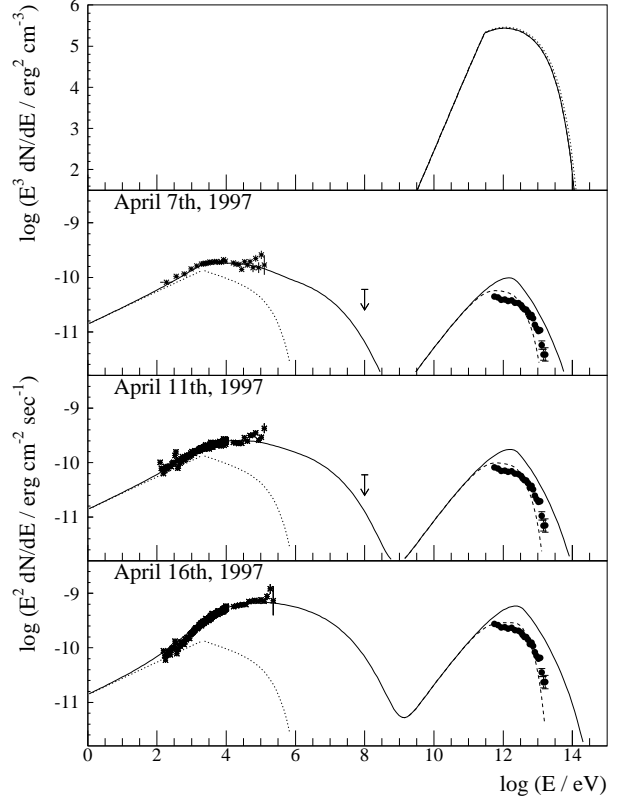


**Figure 11.** Same as in Fig. 7 but for the two-component model with time variable  $\delta_j(t)$  shown in Fig. 10.

Gamma-ray extinction by the Diffuse Extragalactic Background Radiation (DEBRA), compared to earlier work (see Paper I, and also Guy et al. 2000, Vassiliev 2000, Aharonian et al. 2002, and references therein). E.g. the Gamma-ray SEDs of Figs. 7 and 11 are consistent with the LCDM DEBRA model of Primack et al. (2001). In contrast, the model of Fig. 9, implies negligible extinction below  $\sim 10$  TeV. Especially the model with flux variability through the Doppler factor (Fig. 11) can produce very different intrinsic Gamma-ray SEDs while perfectly fitting the X-ray and Gamma-ray flux variations and the X-ray photon indices. In this model, the time variability of X-ray fluxes and energy spectra and TeV Gamma-ray fluxes constrains only the absolute flux level and energy spectrum of the quasi-stationary component, and the relative changes of the Doppler factor. The absolute value of  $\delta_j$ , as well as the parameters  $R$ ,  $B$ , and  $t_{\text{esc}}$  remain degenerate.

An upper limit on the modification of the TeV Gamma-ray energy spectrum by extragalactic extinction can be derived from the fact, that the emitted time averaged Gamma-ray energy spectrum is unlikely to be harder than  $dN_\gamma/dE \propto E^{-\Gamma}$  with  $\Gamma \approx 1.5$ . In Fig. 12 the range of allowed changes of Gamma-ray optical depth with Gamma-ray energy is shown and is compared to recent model calculations of Primack et al. (2001). A more accurate estimate of the amount of extragalactic extinction from SSC modeling of Mrk 501 requires to pin down the jet parameters. Some key-observations are discussed further below; a more detailed discussion will be given by Coppi et al. (2002).

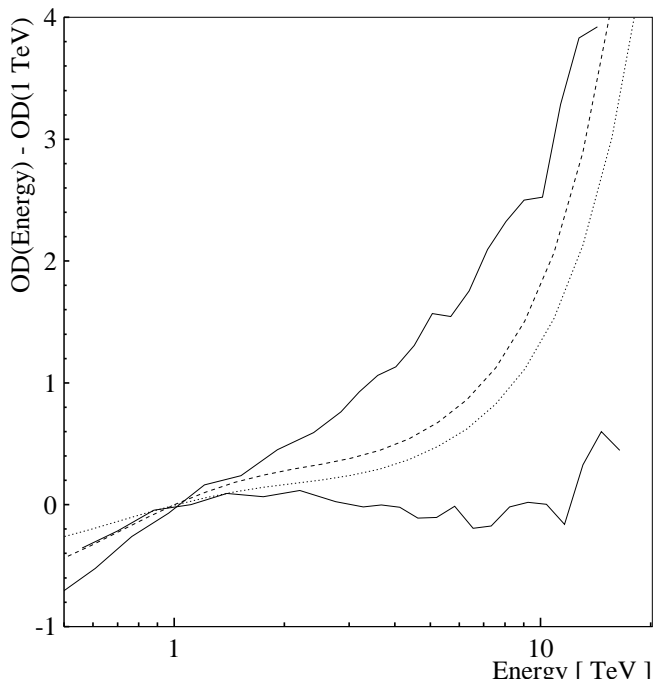


**Figure 12.** Change of GeV/TeV Gamma-ray optical depth as function of Gamma-ray energy, inferred from comparing the model of Fig. 11 (lower solid lines, respectively) with the 1997 time averaged Gamma-ray energy spectrum measured by HEGRA (Aharonian et al. 1999b, 2001a). The upper solid line is an upper limit for parameter combinations for which the 0.5–16 TeV energy spectrum approximates a power law of photon index 1.5. The upper limits include  $2\sigma$  statistical errors and take the 15% uncertainty of the absolute HEGRA energy calibration into account. Allowed DEBRA models have to lie between the two solid lines. However, even if an absorption model lies between the two solid curves it does not imply that a valid SSC model exists such that the absorbed Gamma-ray spectrum describes the data (the solid lines give a necessary but not sufficient condition that a DEBRA model is consistent with the SSC models and the data). The dashed and dotted lines show model predictions of Primack et al. 2001 (“LCDM” with Kennicutt and Salpeter Stellar Initial Mass Functions, respectively). All curves have been normalized to 1 TeV where the systematic errors on the HEGRA energy spectrum are small.

(v) Table 2 lists for all studied models the electron to magnetic field energy density ratio  $r = (u_e / u_B)$  as well as the minimum kinetic luminosity  $L_k = \pi R^2 c \Gamma^2 (u_e + u_B)$  (we use  $\Gamma = \delta_j$ ). All models are strongly out of equipartition with  $r$  between 300 and 7500. Similar results, derived from an one-zone stationary SSC model, have recently been reported by Kino et al. (2002). The kinetic luminosities lie between  $5 \times 10^{42} \text{ erg s}^{-1}$  and  $2 \times 10^{44} \text{ erg s}^{-1}$ , more than 1000 times the emitted luminosity of  $\sim 5 \times 10^{39} \text{ erg s}^{-1}$ . Assuming that the jet has to carry at least a factor of 10 more energy in protons or cold electrons to be able to accelerate the relativistic electrons, it follows that TeV blazars have rather powerful outflows. Models with high  $\gamma_{\text{min}}$ -values are closest to equipartition and require the least power.

In SSC models the X-ray to TeV Gamma-ray luminosity ratio strongly depends on the size and magnetic field of the emission region. As a consequence, most models that have been proposed to account for the flaring activity (as e.g.

the internal shock model of Spada et al. 2001) would not predict the tight correlation of X-ray and TeV Gamma-ray fluxes through a large number of distinct flares as shown in Fig. 1.

The interpretation that a single emission region of constant size produces a series of flares encounters several problems: (i) due to the strong dominance of particle pressure over magnetic field pressure, the emission region should quickly expand adiabatically and thus become undetectable; (ii) it is not clear how the energy required for sustaining a prolonged flaring phase could be fed into the emission region (see above remarks about the poor radiative efficiency of typical SSC models); (iii) during the flaring period that lasted more than  $\Delta t \sim 2$  months, the emission region would have advanced by  $\sim c \Gamma^2 \Delta t$ , that means by a distance of about  $\sim 100$  pc. The stability of the radius of the emission region would thus imply a jet opening angle of  $\sim 10^{-4}^\circ$ , many orders less than radio observations indicate.

In an alternative interpretation, the flares originate from distinct emission regions with similar characteristics, i.e. size and magnetic field. Such emission regions might form as the jet becomes radiative at a certain distance from the central engine. The fact that our models give particle escape times on the order of and shorter than the flux variability time scale indicates that the flare duration is limited by the adiabatic expansion of individual emission regions. The jet would naturally feed energy to the site where the flares originate.

The conclusions presented here are not limited to SSC models. Also in EC models, the tight X-ray/TeV Gamma-ray correlation indicates a preferred location for the production of individual flares: why else should the ratio of the jet frame magnetic field and external seed photon energy densities remain roughly constant during 2 months? The preferred distance from the central engine could correspond to a characteristic length at which the jet becomes unstable. Alternatively, a change in ambient pressure could induce jet instabilities at a certain distance from the central engine. Note that a qualitatively different but similarly puzzling stability has been found in the hardness intensity correlation of Mrk 421 (Fossati et al. 2000) for measurements taken between days and years apart. Our conclusion from this discussion is that refined modeling should treat adiabatic expansion with more detail.

Since the modeling is computationally very intensive, we explored only a limited number of models. E.g. we did not consider EC models which historically have been applied to the more powerful EGRET Blazars. For high jet Doppler factors even a very weak external photon field as e.g., IR radiation from dust, can be boosted and become significant in jet the frame. Depending on the seed photon energy spectrum, the radiative IC cooling of lower energy electrons might be stronger than for high energy electrons due to the Klein-Nishina effect. A possible consequence is that the energy spectra of EC models can be harder than for SSC models for a given value of  $B$ . Thus, the Klein-Nishina effect introduces a very rich behavior of EC models and the consequences of radiative cooling in the extremely “blue” TeV Gamma-ray blazars can substantially differ from those in EGRET GeV blazars.

Crucial advances in fixing model parameters will only be possible by substantially extending the observational cov-

erage in time and wavelength. The 1997 April and May observations had diurnal integration rates of typically 2 times 20 min. Pinning down the evolution of the source during several flares requires quasi-continuous monitoring over many days. Unfortunately, no sensitive X-ray all sky monitor with broadband spectroscopic capabilities will be available for the next several years or even longer. Such an instrument would be able to participate in intensive Multiwavelength campaigns on a large number of objects. The upcoming generation of Cherenkov telescopes CANGAROO III, H.E.S.S., MAGIC, and VERITAS will have energy thresholds of between 10 GeV and 50 GeV and a one order of magnitude higher sensitivity. The lower energy threshold is of crucial importance as it makes it possible to assess the IC component at low energies where extragalactic extinction is negligible ( $z < 0.2$ ) or much less ( $z = 1$ ) than at  $\sim 500$  GeV. The new experiments should be able to reliably assess changes of the diurnal GeV/TeV energy spectra with a statistical and systematic accuracy in photon index of 0.05 or better, due to better Gamma-ray statistics and improved detector calibration and atmospheric monitoring. Thus spectral changes as shown in Figs. 3, 4, and 10 will become measurable.

A key observation for fixing the jet parameters would be to measure a time lag between the X-ray and the TeV Gamma-ray flux variability. A general prediction of SSC models is a time delay of approximately a light crossing time  $R c^{-1}$  between the leading X-ray and following Gamma-ray fluxes. The measurement of this delay would allow one to determine the size of the emission region. The requirement that the DEBRA reduces the 2 TeV flux by a factor of 5 or less would break the degeneracy in  $\delta_j$  and  $B$ . If the X-ray/TeV Gamma-ray lag remains elusive it may be that the determination of the jet parameters of the TeV blazars detected so far has to wait until more reliable DEBRA estimates will be possible based on multiple Blazar detections at redshifts between 0.05 and 1.

**Acknowledgements** The authors thank J. Quinn, D. Kranich, and A. Djannati-Atai for the Whipple, HEGRA CT1, and CAT GeV/TeV data taken during 1997. E. Pian kindly provided us with the BeppoSAX data. We thank M. Böttcher, M. Sikora, J. Kirk, K. Motoki, and A. Celotti for contributing very valuable comments. HK thanks J. Primack for substantial discussion on the Diffuse Extragalactic Background Radiation and for helpful suggestions regarding Fig. 12. HK acknowledges support by NASA (NAS8-39073).

## REFERENCES

- Achterberg A., Gallant Y.A., Kirk J.G., Guthmann, A.W., 2001, MNRAS, 328, 393  
 Aharonian F.A., 2000, New A, 5, 377  
 Aharonian F.A., Akhperjanian A.G., Barrio J.A., et al., 1999a, A&A, 342, 69  
 Aharonian F.A., Akhperjanian A.G., Barrio J.A., et al., 1999b, A&A, 349, 11  
 Aharonian F.A., Akhperjanian A.G., Barrio J.A., et al., 1999c, A&A, 349, 29  
 Aharonian F.A., Akhperjanian A.G., Barrio J.A., et al., 2001, ApJ, 546, 898  
 Aharonian F.A., Akhperjanian A.G., Barrio J.A., et al., 2001, A&A, 366, 62  
 Aharonian F.A., Timokhin A.N., Plyasheshnikov A.V. 2002, A&A, 384, 834  
 Bednarek, W., Protheroe, R.J., 1997, MNRAS, 292, 646  
 Bednarek, W., Protheroe, R.J., 1999, MNRAS, 310, 577  
 Bell A.R., 1978, MNRAS, 182, 147  
 Bell A.R., 1987, MNRAS, 225, 615  
 Bicknell G.V., Wagner S.J., Groves B., 2001, In: Procs. of the International Symposium on Gamma-Ray Astronomy, Heidelberg, June 2000, eds F. Aharonian and H. Völk, AIP 558, p. 261  
 Blandford R.D., Ostriker J.P., 1978, ApJ, 221, L29  
 Błażejowski M., Sikora M., Moderski R., Madejski G.M., 2000, ApJ, 545, 107  
 Böttcher M., Mause H., Schlickeiser R., 1997, A&A, 324, 395  
 Buckley J.H., Akerlof C.W., Biller S., et al., 1996, ApJ, 472, L9  
 Catanese M., Bradbury S.M., Breslin A.C., et al., 1997, ApJ, 487, L143  
 Chiaberge M., Capetti A., Celotti, A., A&A, 349, 77  
 Chiaberge M., Ghisellini G., 1999, MNRAS, 306, 551  
 Coppi P.S. 1992, MNRAS, 258, 657  
 Coppi P.S., Aharonian F. A., 1999, ApJ, 521, L33  
 Coppi P.S., Blandford R.D., 1990, MNRAS, 245, 453  
 Coppi P.S., Krawczynski H., Aharonian F., in preparation.  
 Dar A., Laor A., 1997, ApJ, 478, L5  
 Dermer C.D., Li H., Chiang J., 1998, In: "The Extreme Universe," 3rd INTEGRAL Workshop, 14-18 September 1998, Taormina, Italy  
 Djannati-Atai A., Piron F., Barrau A., et al., 1999, A&A, 350, 17  
 Fossati G., Celotti A., Chiaberge M., et al., 2000, ApJ, 541, 166  
 Gaidos J.A., Akerlof C.W., Biller S.D., et al., 1996, Nat, 383, 319  
 Ghisellini, G., Celotti, A., Fossati, G., Maraschi, L., Comastri, A., 1998, MNRAS, 301, 451  
 Gould J., Schröder G., 1966, Phys. Rev. Lett. 16, 252  
 Guy J., Renault C., Aharonian F.A., Rivoal M., Tavernet J.-P., 2000, A&A, 359, 419  
 Hartman R.C., Bertsch D.L., Bloom S.D., 1999, ApJS, 123, 79  
 Hartman, R.C., Böttcher, M., Aldering, G., et al., 2001, ApJ, 553, 683  
 Hoshino M., Arons J., Gallant Y.A., Langdon A.B., 1992, ApJ, 390, 454  
 Inoue S., Takahara F., 1996, ApJ, 463, 555  
 Kataoka J., Takahashi T., Makino F., et al., 2000, ApJ, 528, 243  
 Kirk J.G., Duffy P., 1999, J. Phys. G, 25, R163  
 Kirk J.G., Guthmann A.W., Gallant Y.A., Achterberg A. 2000, ApJ, 542, 235  
 Kirk J.G., Rieger F.M., Mastichiadis A., 1998, A&A, 333, 452  
 Kirk J.G., Mastichiadis A., 1999, APh, 11, 45  
 Konopelko A.K., Kirk J.G., Stecker F.W., Mastichiadis A., 1999, ApJ, 518, L13  
 Krawczynski H., Coppi P.S., Maccarone T., Aharonian F., 2000, A&A, 353, 97  
 Kusunose, M., Takahara, F., Li, H., 2000, ApJ, 536, 299  
 Levinson A., 1996, MNRAS, 278, 1018  
 Mannheim K., 1993, Science, 279, 684  
 Mastichiadis A., Kirk J.G., 1997, A&A, 320, 19  
 Mattox J. R., Wagner S.J., Malkan M., 1997, ApJ, 476, 692  
 McClements K.G., Dendy R.O., Bingham R., Kirk J.G., Drury L.O'C., 1997, MNRAS, 291, 241  
 Mücke A., Protheroe R.J., 2000, In: "GeV-TeV Astrophysics: Toward a Major Atmospheric Cherenkov Telescope VI", eds. B.L. Dingus, M.H. Salamon & D.B. Kieda, Snowbird, Utah (August 1999), AIP 515, 149  
 Petry D., Böttcher M., Connaughton V., et al., 2000, ApJ, 536, 742  
 Pian E., Vacanti G., Tagliaferri G., et al., 1998, ApJ, 492, L17  
 Pohl M., Schlickeiser R., 2000, A&A, 354, 395  
 Primack J.R., Somerville R.S., Bullock J.S., Devriendt J.E.G.,

- 2001, In: Procs. of the International Symposium on Gamma-Ray Astronomy, Heidelberg, June 2000, eds F. Aharonian and H. Völk, AIP 558, p. 463
- Quinn J., Bond I.H., Boyle P.J., 1999, ApJ, 518, 693
- Sambruna R., Aharonian F.A., Krawczynski H., et al., 2000, ApJ, 538, 127
- Sikora M., Błażejowski M., Begelman M.C., Moderski R., 2001, ApJ, 554, 1
- Spada M., Ghisellini G., Lazzati D., Celotti A., 2001, MNRAS, 325, 1559
- Stecker F.W., De Jager O.C., Salamon M.H., 1992, ApJ, 390, L49
- Takahashi T., Tashiro M., Madejski G., et al., 1996, ApJ, 470, L89
- Tevecchio F., Maraschi L., Pian E., et al., 2001, ApJ, 554, 725
- Ulrich M.H., Maraschi L., Urry C.M., 1997, ARA&A, 35, 445
- Vassiliev V.V., APh., 12, 217
- Wagner S., von Montigny C., Herter M., In: Procs. of the 4th Compton Symposium at Williamsburg, VA
- Wehrle A.E., Pian E., Urry C.M., et al., 1998, ApJ, 497, 178

**Table 1.** Selected Blazar SSC Models relevant to this paper

Authors	Objects Studied	Time Dependent?	SED Peak Determined By	Flare Mechanism
Inoue & Takahara (1996)	3C 279, Mrk 421	No	Cooling vs. Particle Escape	Not specified
Bednarek & Protheroe (1997; 1999)	Mrk 421, Mrk 501	No	Not specified	Not specified
Böttcher et al. (1997)	Mrk 421	No	$\gamma_{\min}$	$B, \gamma_{\min}$
Mastichiadis & Kirk (1997)	Mrk 421	Yes	Cooling vs. Particle Escape	$Q_0, \gamma_{\max}, B$
Pian et al. (1997)	Mrk 501	No	$\gamma_{\min}$	$\gamma_{\min}, \gamma_{\max}$
Dermer et al. (1998)	generic	Yes	Cooling vs. Particle Escape and Plasmon Deceleration	$\delta_j$
Chiaberge & Ghisellini (1999)	generic	Yes	Cooling vs. Particle Escape	$Q_0$
Coppi & Aharonian (1999)	generic	Yes	Cooling vs. Particle Escape	$Q_0, B$
Kirk & Mastichiadis (1999)	generic	Yes	Cooling vs. Particle Escape	$Q_0$
Kataoka et al. (2000)	PKS 2155-304	Yes	Cooling vs. Particle Escape	$\gamma_{\max}$
Petry et al. (2000)	Mrk 501	No	Cooling vs. Injection Time Scale	$p$
Kusunose et al. (2000)	generic	Yes	Cooling vs. Particle Escape	$\gamma_{\max}$ (through $t_{\text{esc}}$ and $t_{\text{acc}}$ )
Tavecchio et al. (2001)	Mrk 501	No	Not specified	Change of $\gamma_b$
Krawczynski et al. (2001)	Mrk 421	Yes	Cooling vs. Particle Escape	$\gamma_{\max}$
Sikora et al. (2001)	3C 279, PKS 1406-076	Yes	Cooling vs. Injection Time Scale or $\gamma_{\min}$	$Q_0$
Kino et al. (2002)	Mrk 421, Mrk 501, PKS 2155-304	No	Cooling vs. Particle Escape	Not specified
This work	Mrk 501	Yes	Cooling vs. Particle Escape or $\gamma_{\min}$	$Q_0, \gamma_{\max}, \delta_j$

**Table 2.** Parameters of Models Shown in Figures

Time Dependent Parameter	Comments	$\bar{\delta}_j$	$R$ [cm]	$\log_{10} (B/1 \text{ G})$	$t_{\text{esc}} [R c^{-1}]$	$\gamma_{\min}$	$\gamma_{\max}$	$\xi$	$\eta$	$u_e/u_B$	$L_k [\text{erg s}^{-1}]$
$Q_0(t)$	1-component	45	$1.1 \times 10^{16}$	-1.85	10	1000	$2.5 \times 10^7$	0.5	0.2	660	$1.2 \times 10^{44}$
$\gamma_{\max}(t)$	1-component	45	$1.5 \times 10^{16}$	-2.05	3	1000	$1.6\text{-}25 \times 10^6$	0.5	0.2	1200	$1.7 \times 10^{44}$
$\gamma_{\max}(t) \propto Q_0(t)^2$	1-component	45	$3.2 \times 10^{15}$	-1.45	3	1000	$1.6\text{-}6.3 \times 10^6$	0.5	0.1	860	$8.3 \times 10^{43}$
$Q_0(t)$	2-component	45	$3.4 \times 10^{15}$	-1.85	3	1000	$2.3 \times 10^7$	0.5	0.4	7470	$1.3 \times 10^{44}$
$Q_0(t)$	2-component, high $\gamma_{\min}$	45	$4.5 \times 10^{13}$	0.05	10000	$1.0 \times 10^5$	$1.4 \times 10^7$	0.5	0.00	290	$5.6 \times 10^{42}$
$\delta_j(t)$	2-component, high $\gamma_{\min}$	10	$10^{15}$	-0.8	10	$4.5 \times 10^5$	$2.9 \times 10^7$	0.5	0.04	2970	$2.8 \times 10^{43}$